A Time-Weighted Dynamic Time Warping Method for Land-Use and Land-Cover Mapping

Article *in* IEEE Journal of Selected Topics in Applied Earth Observations and Remote Sensing · August 2016

DOI: 10.1109/JSTARS.2016.2517118

A Time-Weighted Dynamic Time Warping Method for Land-Use and Land-Cover Mapping

Victor Maus, *Member, IEEE*, Gilberto Câmara, Ricardo Cartaxo, Alber Sanchez, Fernando M. Ramos, and Gilberto R. de Queiroz

***Abstract*—This paper presents a time-weighted version of the dynamic time warping (DTW) method for land-use and land-cover classification using remote sensing image time series. Methods based on DTW have achieved significant results in time-series data mining. The original DTW method works well for shape matching, but is not suited for remote sensing time-series classification. It disregards the temporal range when finding the best alignment between two time series. Since each land-cover class has a specific phenological cycle, a good time-series land-cover classifier needs to balance between shape matching and temporal alignment. To that end, we adjusted the original DTW method to include a temporal weight that accounts for seasonality of land-cover types. The resulting algorithm improves on previous methods for land-cover classification using DTW. In a case study in a tropical forest area, our proposed logistic time-weighted version achieves the best overall accuracy of 87.32%. The accuracy of a version with maximum time delay constraints is 84.66%. A time-warping method without time constraints has a 70.14% accuracy. To get good results with the proposed algorithm, the spatial and temporal resolutions of the data should capture the properties of the landscape. The pattern samples should also represent well the temporal variation of land cover.**

***Index Terms*—Dynamic programming, image sequence analysis, monitoring, pattern classification, time series.**

I. Introduction

THERE is a global increase in food and energy production from agriculture to keep 7.3 billion people. To support sustainable practices and find out about unsustainable uses of natural resources, good quality land-use and land-cover datasets are essential [1]. Earth observation satellites are the only source that provides a continuous and consistent set of information about the Earth's land and oceans. Since remote sensing satellites revisit the same place repeatedly, we can calibrate their images so that measures of the same place in different times are comparable. These observation can be organized in regular time intervals, so that each measure from sensor is mapped into a three-dimensional (3-D) array in space-time.

From a data analysis perspective, researchers then have access to space-time datasets. This has lead to much recent research on satellite image time-series analysis. Algorithms for analyzing image time series include methods for time-series reconstruction [2], detecting trend and seasonal changes [3]–[5], extracting seasonality information [6], land-cover mapping [7], detecting forest disturbance and recovery [8]–[10], crop classification [11]–[13], planted forest mapping [14], and crop expansion and intensification [15], [16].

Research on time-series data mining shows that methods based on dynamic time warping (DTW) have achieved significant results in many applications [17]–[19]. DTW works by comparing a temporal signature of a known event (e.g., a person's speech) to an unknown time series (e.g., a speech record of unknown origin) [17], [20]–[23]. The algorithm compares two time series and finds their optimal alignment, providing a dissimilarity measure as a result [23]. DTW provides a robust distance measure for comparing time series, even if they are irregularly sampled [13] or are out of phase in the time axis [24]. The large range of applications of digital time warping for time series analysis motivated our idea of using DTW for remote sensing applications.

The DTW method works well for shape matching, but is not suited *per se* for remote sensing time-series classification. It disregards the temporal range when finding the best alignment between two time series [23], [25]. Each land-cover class has a distinct phenological cycle that is relevant for space-time classification [26], [27]. Therefore, a good time-series land-cover classifier needs to balance between shape matching and temporal alignment. For example, although crops tend to vary their annual phenological cycles, these variations will not be extreme. Consider a set of samples of soybean whose cycles range from 90 to 120 days. A time series with similar shape but with much larger cycle is unlikely to come from a soybean crop. The standard DTW method warps time to match the two series. To avoid such mismatches, we introduce a time constraint that helps to distinguish between different types of land-use and land-cover classes.

Recent papers by [13] and [28] have used DTW for satellite image time-series classification. The method proposed in these papers sets a maximum time delay to avoid inconsistent temporal distortions based on the date of the satellite images. The time series is split in 1 year segments to match the agricultural phenological cycle in Europe. However, this temporal

Manuscript received July 08, 2015; revised November 06, 2015; accepted January 07, 2015. Part of this work was developed in the Young Scientists Summer Program at the International Institute for Systems Analysis, Laxenburg (Austria). This work was supported in part by the Institute for Geoinformatics, University of Münster (Germany), and in part by the Earth System Science Center, National Institute for Space Research (Brazil). The work of G. Camara's was supported by CAPES under Grant 23038.0075692012-16, FAPESP e-science program under Grant 2014-08398-6, and CNPq under Grant 3121512014-4.

V. Maus and G. Câmara are with the National Institute for Space Research, 12227010 São José dos Campos, Brazil, and also with the Institute for Geoinformatics, University of Münster, 48149 Münster, Germany (e-mail: vwmaus1@gmail.com).

R. Cartaxo, A. Sanchez, F. M. Ramos, and G. R. de Queiroz are with the National Institute for Space Research, 12227010 São José dos Campos, Brazil.

Color versions of one or more of the figures in this paper are available online at http://ieeexplore.ieee.org.

Digital Object Identifier 10.1109/JSTARS.2016.2517118

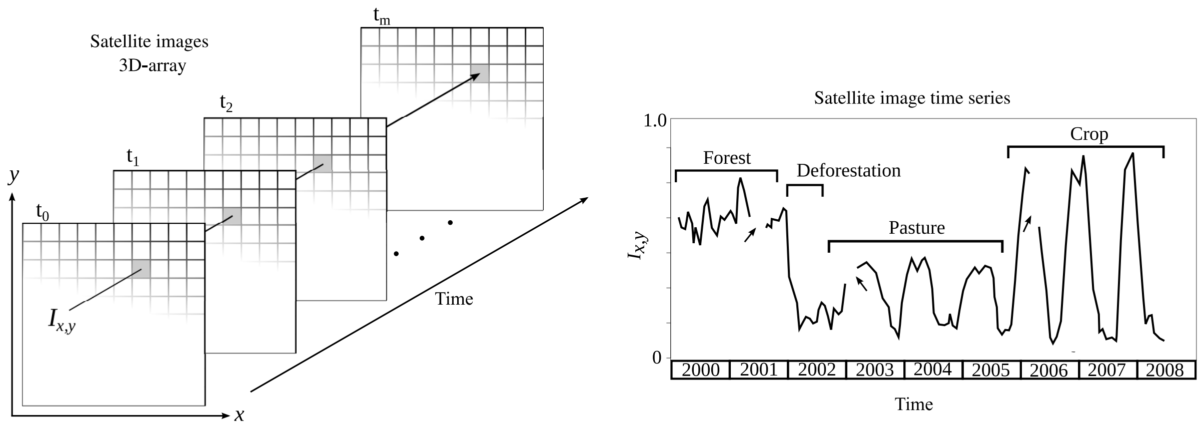

(a) (b)

Fig. 1. (a) 3-D array of satellite images. (b) Vegetation index time series I at the pixel location (x, y). Arrows indicate data gaps.

segmentation reduces the power of the DTW classifier. Crops with phenological cycles longer than 1 year or taking place in different seasons may not be detected. The time-weighted extension to the DTW algorithm avoids this problem. Temporal segments of a remote sensing time series are classified without splitting them into fixed parts. This method is flexible to account for multiyear crops, single cropping, and double cropping. It is also robust to account for other land-cover types such as forest and pasture and works with a small amount of training samples.

Our main contribution is to show that a data mining method such as DTW, when used for land-use and land-cover classification of remote sensing time series, benefits from a temporal constraint. This conjecture has been validated in a case study in the Brazilian Amazon, where we compared the result of our proposed method with other time-warping classifiers.

II. Methods

Since remote sensing satellites cycle the Earth at regular intervals, their data are mappable to 3-D arrays in space-time [Fig. 1(a)]. Each pixel location (x, y) in consecutive times, $t_1, \ldots, t_m$, makes up a satellite image time series, such as the one in Fig. 1(b). From these time series, we can extract land-use and land-cover information. In the example, during the first 2 years the area was covered by forest. It was deforested in 2002. The area was then used for cattle raising (pasture) for 3 years. From 2006 to 2008, it was used for crop production.

Let $\mathbf{V}_{x,y} = (v_1, v_2, \ldots, v_m)$ be a time series of a pixel location (x, y) in consecutive times, $t_1, \ldots, t_m$, where v_i is the value of the sensor measure at time t_i. Combining all the satellite's spatial coverage, we get a set of time series $\mathcal{S} = \{\mathbf{V}_1, \mathbf{V}_2, \ldots, \mathbf{V}_s\}$. We assume that there is a temporal continuity for each land use classes, resulting from human actions. A forest area does not change to grassland or to soybeans overnight. Land-use changes take time. Our hypothesis is that it is possible to associate closed intervals of each time series $\mathbf{V}_{x,y}$ to a specific land-use and land-cover type. For example, suppose a 10-year period where in the first 5 years the area was covered by forest. The area was then used for cattle raising (pasture) for 2 years. After that, it was used for soybean production for 3 years. We want to associate each of these intervals with one of our land classes.

Optical remotely sensed data are affected by cloud cover that introduces a large amount of noise in satellite image time series, as shown in Fig. 1(b). Inter-annual climate variability also changes the phenological cycles of the vegetation, resulting in time series whose periods and intensities do not match on an year-to-year basis [26]. To associate intervals of a satellite image time series with land-cover and land-use classes, we need methods suitable for noisy and out-of-phase time series. We chose the DTW algorithm because it is suitable for this problem.

The papers by [13] and [28] applied the DTW algorithm to classify intervals of satellite image time series, such as in Fig. 2(a). In this case, two time series have approximately the same length and the first and last points in both time series must match. In practice, crop phenological cycles can vary in an year-to-year basis, depending on climate conditions and land management. Examples include shifting the greenup and dormancy stages of the vegetation [26], [27]. To avoid possible inconsistent matching of phenological cycles caused by splitting the time series, we use an open boundary version of DTW, Fig. 2(b). The open boundary method does not require two time series to be of the same length, and it is suitable to find all possible matches of one pattern within a long-term time series [29].

The open boundary DTW algorithm disregards the time dimension and can cause inconsistent phase alignments, e.g., a winter crop template can match the shape of a summer crop. To avoid these temporal inconsistencies, we introduce a temporal constraint. If there is a large seasonal difference between the sample pattern and its match in time series, an extra cost is added to the DTW distance measure. This constraint controls the time warping and makes the time-series alignment dependent on the seasons. This is especially useful for detecting temporary crops and for distinguishing pasture from agriculture.

Classification using open boundary DTW [29] requires matching subsequences of the time-series associated with

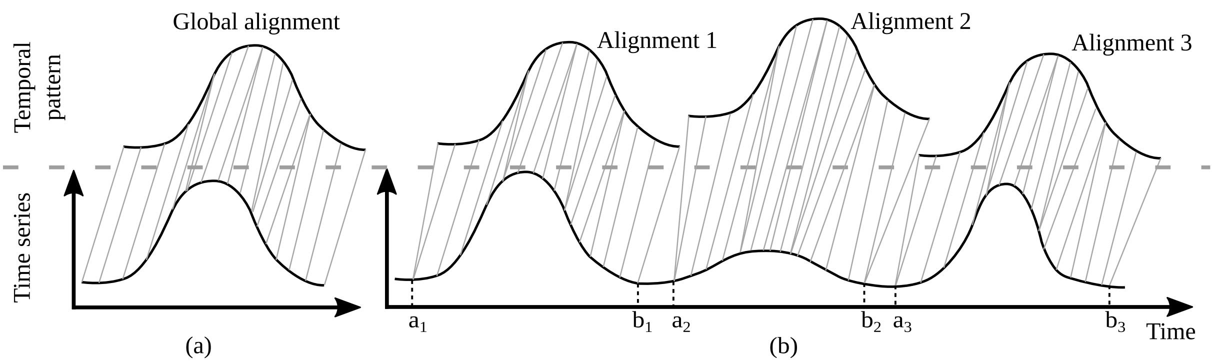

Fig. 2. (a) DTW alignment between two time series with approximately same length. (b) DTW alignments between a pattern whose length is much shorter than the time series. Indexes a and b are starting points and ending points of each interval in the long-term time series, respectively.

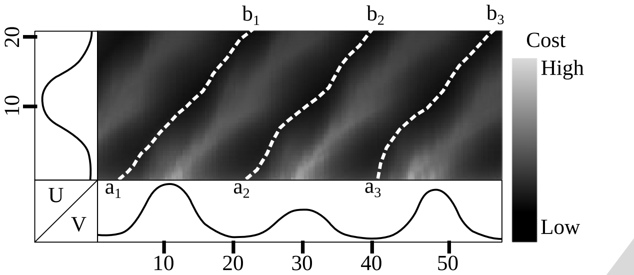

Fig. 3. Accumulated cost matrix $\mathcal{D}$ showing three possible alignment of the pattern $\mathbf{U}$ within the long-term time series $\mathbf{V}$. Indexes a are starting points and b ending points of each DTW alignment in $\mathbf{V}$.

each pixel location to samples of the expected classes. For each class c, we take a set of time-series samples $\mathcal{Q}_c = \{\mathbf{U}_1, \mathbf{U}_2, \ldots, \mathbf{U}_q\}$, where $\mathbf{U} = (u_1, \ldots, u_n)$ is a time series with $n \ll m$ (i.e., the pattern length is much shorter than the sensor time series $\mathbf{V}$). q is the number of patterns for each class. These samples are then used to classify the intervals of the time series $\mathbf{V} \in \mathcal{S}$.

The classification is done for each pixel with two steps. 1) The DTW algorithm is applied for each pattern in $\mathcal{Q}$ and each time series $\mathbf{V} \in \mathcal{S}$. This step provides information on how patterns match intervals of the time series. 2) The best DTW matches are used to build a sequence of land-use and land-cover maps.

A. Step 1: DTW Alignment

The DTW alignment starts by computing a $n \times m$ matrix Ψ, whose elements $\psi_{i,j}$ are the absolute difference between $u_i \in \mathbf{U} \; \forall \, i = 1, \ldots, n$ and $v_j \in \mathbf{V} \; \forall \, j = 1, \ldots, m$. From Ψ, we compute an accumulated cost matrix $\mathbf{D}$ by a recursive sum of the minimal distances, such that

$$d_{i,j} = \psi_{i,j} + min\{d_{i-1,j}, d_{i-1,j-1}, d_{i,j-1}\} \tag{1}$$

that is subject to the following boundary conditions:

$$d_{i,j} = \begin{cases} \psi_{i,j}, & i = 1, \quad j = 1 \\ \sum_{k=1}^{i} \psi_{k,j}, & 1 < i \le n, \quad j = 1 \\ \sum_{k=1}^{j} \psi_{i,k}, & i = 1, \quad 1 < j \le m. \end{cases} \tag{2}$$

Fig. (3) shows an example of the accumulated cost matrix $\mathbf{D}$. Intuitively, the DTW alignment runs along the "valleys" of low cost in the accumulated cost matrix $\mathbf{D}$, that has as many "valleys" as the number of matches between $\mathbf{U}$ and $\mathbf{V}$. The kth low-cost path in $\mathbf{D}$ produces an alignment between the pattern and a subsequence $\mathbf{V}|_{a_k}^{b_k}$ with associated DTW distance δ_k, where a_k is the starting point and b_k the ending point of the subsequence k [29], as shown in Fig. (3).

Each minimum point in the last line of the accumulated cost matrix, i.e., $d_{n,j} \; \forall \; j = 1, \ldots, m$, produces an alignment, with b_k and the δ_k given by

$$b_k = argmin_k(d_{n,j}), \quad k = 1, \ldots, K \tag{3}$$

$$\delta_k = d_{n,b_k} \tag{4}$$

where K is the number of minimum points in last line of the accumulated cost matrix.

A reverse algorithm, (5), maps the warping path $\mathbf{P}_k = (p_1, \ldots, p_L)$ along the kth low-cost "valley" in $\mathbf{D}$. The algorithm starts in $p_{l=L} = (i = n, j = b_k)$ and ends when $i = 1$, i.e., $p_{l=1} = (i = 1, j = a_k)$, where L denotes the last point of the alignment. The warping path $\mathbf{P}_k$ contains the matching points between the time series. Note that the backward step in (5) implies the monotonicity condition [21], [29], i.e., the alignment preserves the order of the time series

$$p_{l-1} = \begin{cases} (i, a_k = j), & \text{if} \quad i = 1 \\ (i-1, j), & \text{if} \quad j = 1 \\ argmin(d_{i-1,j}, & \\ \qquad d_{i-1,j-1}, & \text{otherwise.} \\ \qquad d_{i,j-1}) & \end{cases} \tag{5}$$

The original DTW algorithm does not account for the phase difference between two time series [25]. However, land-use and land-cover types have distinct phenological cycles that are relevant for space-time classification [26], [27]. We introduce a time-weighted extension of DTW (TWDTW), based on the date of each pixel in the satellite image. This time-weighted version of DTW adds a temporal cost ω to the cost matrix Ψ, whose elements become $\psi_{i,j} = |u_i - v_j| + \omega_{i,j}$. To compute the temporal cost we propose both a linear

$$\omega_{i,j} = g(t_i, t_j) \tag{6}$$

and a logistic model with midpoint β, and steepness α, such that

$$\omega_{i,j} = \frac{1}{1 + e^{-\alpha(g(t_i,t_j) - \beta)}} \tag{7}$$

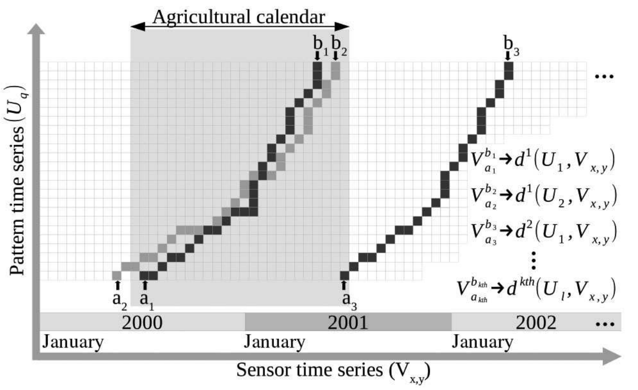

Fig. 4. Open boundary DTW alignment. Dark and light shades represent the alignments of the patterns U_1 and U_2, respectively. Indexes a_k and b_k represent the starting and ending points of the kth alignment in $\mathbf{V}$ associated with a DTW distance measure δ_k.

where $g(t_i, t_j)$ is the elapsed time in days between the dates t_i in the pattern and t_j in the time series. We ran many tests using different values of β and α. We then used the best global accuracy performance to set the parameters for the logistic TWDTW.

B. Step 2: Map Building

The DTW algorithm matches each pattern to the input time series independently from the others. Thus, each interval of the time series $\mathbf{V}$ can fit different patterns. To associate an interval of the time series $\mathbf{V}$ to a land-cover and land-use class, we choose the best fitting pattern, i.e., the pattern with the lowest DTW distance in the interval. After finding the best fit, we can produce maps that show a land-cover and land-use classification for a given period.

To compare our results with other land-use/cover products, we produced maps matching the agricultural calendar from July to June (gray area in Fig. 4). We find the pattern that has the lowest DTW distance to a subsequence $\mathbf{V}|_{a_k}^{b_k}$ partly contained in the crop calendar. Fig. 4 shows the matching of two patterns, $\mathbf{U}_1$ and $\mathbf{U}_2$, that are partially in the same agricultural year from July 2000 to June 2001. In this case, we pick the one with the lowest DTW distance, i.e., the most similar pattern for that period.

III. Experiments

In our experiments, we tested the performance of four different DTW methods: 1) the original DTW algorithm without time constraints (i.e., $\omega = 0$); 2) DTW with maximum time delay as proposed by [13]; 3) linear TWDTW; and 4) logistic TWDTW.

We used time series of enhanced vegetation index (EVI) from July 2000 to June 2013 based on moderate resolution imaging spectroradiometer (MODIS) product MOD13Q1 16 day 250 m. MODIS EVI has improved sensitivity in high-biomass regions through a canopy background adjustment and a reduction in the atmosphere influences [30], [31].

The EVI time series is subject to atmospheric effects, such as cloud cover and path radiance from aerosols [32]. To reduce the spurious oscillation due to atmospheric effects, we apply a discrete wavelet decomposition [33] and then filter the time series by removing the highest wavelet frequency. The wavelet filter preserves the essential temporal variation and is more sensitive to vegetation seasonal changes than filters based on Fourier transform [34].

An important scientific problem to the authors is understanding changes in the Brazilian Amazonian rain forest, which has an area of 4 100 000 km^2. In Amazonia, 720 000 km^2 have been deforested since the 1970s [35]. In the Copenhagen Climate Conference in 2009, Brazil pledged to reduce deforestation in Amazonia by 80% relative to the average of the period 1996–2005. Brazil is making good this pledge. Forest cuts in Amazonia fell from 27 700 km^2 in 2004 to 4900 km^2 in 2012, decreasing by 83%. Given the impact of land changes in Amazonia on global biodiversity, emissions, and ecological services, it is important to understand what causes forest removal [36]. INPE (Brazil's National Institute for Space Research) and EMBRAPA (Brazils Agricultural Research Agency) mapped the land use of the deforested areas in Amazonia up to 2008 [37]. Their results show that 63% of the forest cuts are now used for cattle raising. Cattle ranches in Amazonia use extensive practices, with less than 1 head of cattle per hectare. Cash crop agriculture accounts for only 4% of the deforestation. Moreover, more than 20% of the area has been abandoned and is now regrowing as secondary vegetation. To achieve further gains in reducing deforestation and biodiversity loss, we need to understand the different land-use trajectories, including the deforestation dynamics, land-use intensification, and land-abandonment pathways.

We ran a case study in an area in Amazonia that had strong deforestation and cropland expansion in the last decade. We selected the Porto dos Gaúchos municipality that covers approximately 7000 km^2 and is located in the state of Mato Grosso, Brazil, inside of the Amazon Biome. In 2013, its total deforested area was 3023.6 km^2, i.e., 42.9% of the original forest cover [35]. The cropland area grew from 59.8 km^2 in 2000 to 580.8 km^2 in 2013 [38]. We chose the most important classes for that area: forest, secondary vegetation, pasture, single cropping, and double cropping. These classes are the most relevant ones for our study on trajectories of change in Amazonia.

Our classification method requires a set of temporal patterns of the chosen land-use/cover classes. We defined the temporal patterns of forest, pasture, single cropping, and double cropping based on the paper by [39], that presented typical temporal patterns of EVI for different crops types and natural vegetation for the same region of our case study. Reference [39] used several ground truth data collections identified through field studies to derive their averaged EVI signal according to the agricultural calendar from July to June. Here, we joined some of the temporal patterns from [39], such that "soybean" and "cotton" are used as "single cropping," and "soybean–cotton" and "soybean–maize" are "double cropping." We kept the classes "forest" and "pasture." Therefore, each class has one or two patterns shown in Fig. 5.

IV. Results

To assess our algorithm, we used 40 random selected spatial locations from that we could classify 489 samples out of 560 in the period from 2001 to 2014. Most of the unclassified

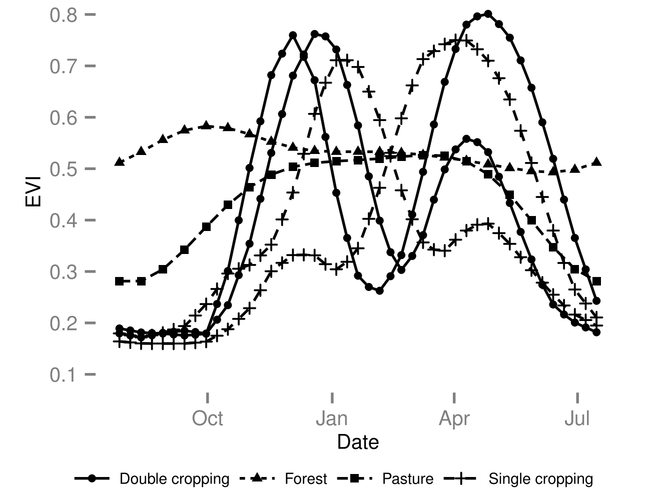

Fig. 5. Temporal patterns of EVI MODIS 16 days. Adapted from [39].

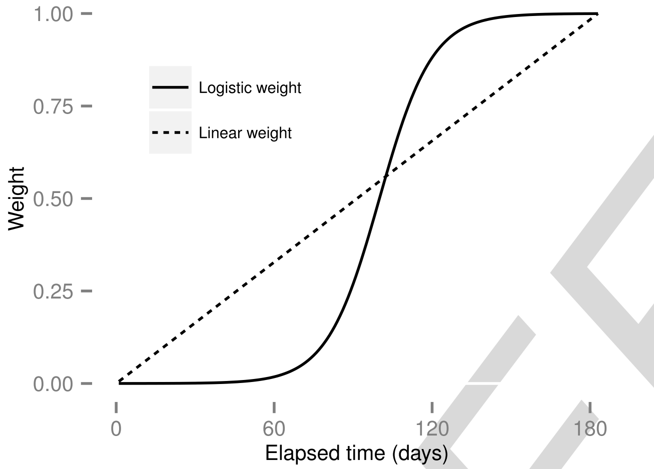

Fig. 6. Linear and logistic time weight. The logistic weight has midpoint $\beta =$ 100 days and steepness $\alpha = 0.1$.

samples had cloud contamination during the growing cycles of single and double cropping because the rainy season in Mato Grosso state is usually from November to March [40]. The samples were classified by visual interpretation of Landsat images using the Google Earth Engine [41]. To separate our classes, we used a set of images corresponding to the agricultural year from July to June. For each year, we used at least four images showing different phenological stages of the vegetation that allow us to distinguish: forest, pasture, single cropping, and double cropping.

The logistic TWDTW had the best performance for $\alpha = 0.1$ and $\beta = 100$ days (global accuracy 87.32%), meaning a low penalty for time warps smaller then 60 days and significant costs for bigger time warps (Fig. 6). In the algorithm proposed by [13], we tested maximum time delays ranging from 30 to 130 days, and found the best performance when the delay was set to 100 days with global accuracy 84.66%. The linear TWDTW had global accuracy 81.6% and the DTW without time restrictions only 70.14%.

Part of the good performance of TWDTW comes from good quality sample patterns. Given a good set of samples, TWDTW uses the length of each pattern as a temporal constraint in its distance measure. The standard version of DTW reduces or enlarges the pattern without temporal restrictions to find the best fit. Unrestricted warping works well for highly variable signals such as speech, but has problems dealing with structured patterns such as land-cover signals. To compare DTW without time constraints and TWDTW, see Fig. 7. In this figure, we show how the best matches for samples patterns of four classes (forest, pasture, single cropping, and double cropping) for the two versions of DTW (with and without time constraints). The DTW without time constraints, Fig. 7(a) overfits the patterns of forest, pasture, and single cropping. The forest and pasture signals are strongly shortened and the single cropping signal is mapped to the first cycle of a double cropping event. By contrast, TWDTW keeps the temporal consistency for all land classes, as shown in Fig. 7(b).

Table I shows the accuracy assessment of the four DTW approaches based on 489 reference samples classified from the Landsat images. In general, the logistic TWDTW had higher accuracy than the other approaches. Although the logistic TWDTW had lower *user's accuracy* than the linear TWDTW for double cropping and forest, its *producer's accuracy* was higher than the linear TWDTW for these classes (cf. Table I). This means that the logistic TWDTW classified more ground truth pixels as such, but with a slightly lower confidence than the linear TWDTW for pixels classified as double cropping and forest. The logistic TWDTW had the same value of sensitivity for double cropping as the maximum delay DTW (i.e., *producer's accuracy* 90.43%), but with larger confidence for this class, *user's accuracy* 92.04% in comparison to 88.89%.

The confusion matrices of the four DTW approaches are shown in Table II. We see that DTW without time restriction had the worst results, particularly, for double cropping that had 57 pixels classified as single cropping. The linear TWDTW classified 24 pixels of double cropping and 34 pixels of pasture as single cropping, and therefore, its confidence for single cropping was only 60.27% (cf. Table I). The logistic TWDW classified 10 pixels of double cropping and 18 pixels of pasture as single cropping, which means a higher confidence than the linear TWDTW classification for single cropping, 75.00%. These results of the logistic TWDW were similar to the results obtained using the maximum time delay DTW, which classified 9 pixels of double cropping and 18 pixels of pasture as single cropping. However, the logistic TWDTW had higher sensitivity than the maximum time delay DTW (84.85% in comparison to 75.76% cf. Table I), that classified 11 pixels as double cropping, 6 as pasture and unclassified other 7 pixels out of 99 pixels of single cropping.

We also compared the accuracy of our classification and the MODIS land cover collection 5, Plant Functional Type (PFT) 500 m [42] using the validation points. Mapping from MODIS classes to our classes is shown in Table III. Originally, the study area was covered by forest. Therefore, the other land-cover types that appear later result from human activities. We aggregated the MODIS categories of trees to a class called forest. We also assume that MODIS shrubland and grassland classes are used as pastureland for cattle raising, and the categories of cereal crops and broad-leaf crops are aggregated to

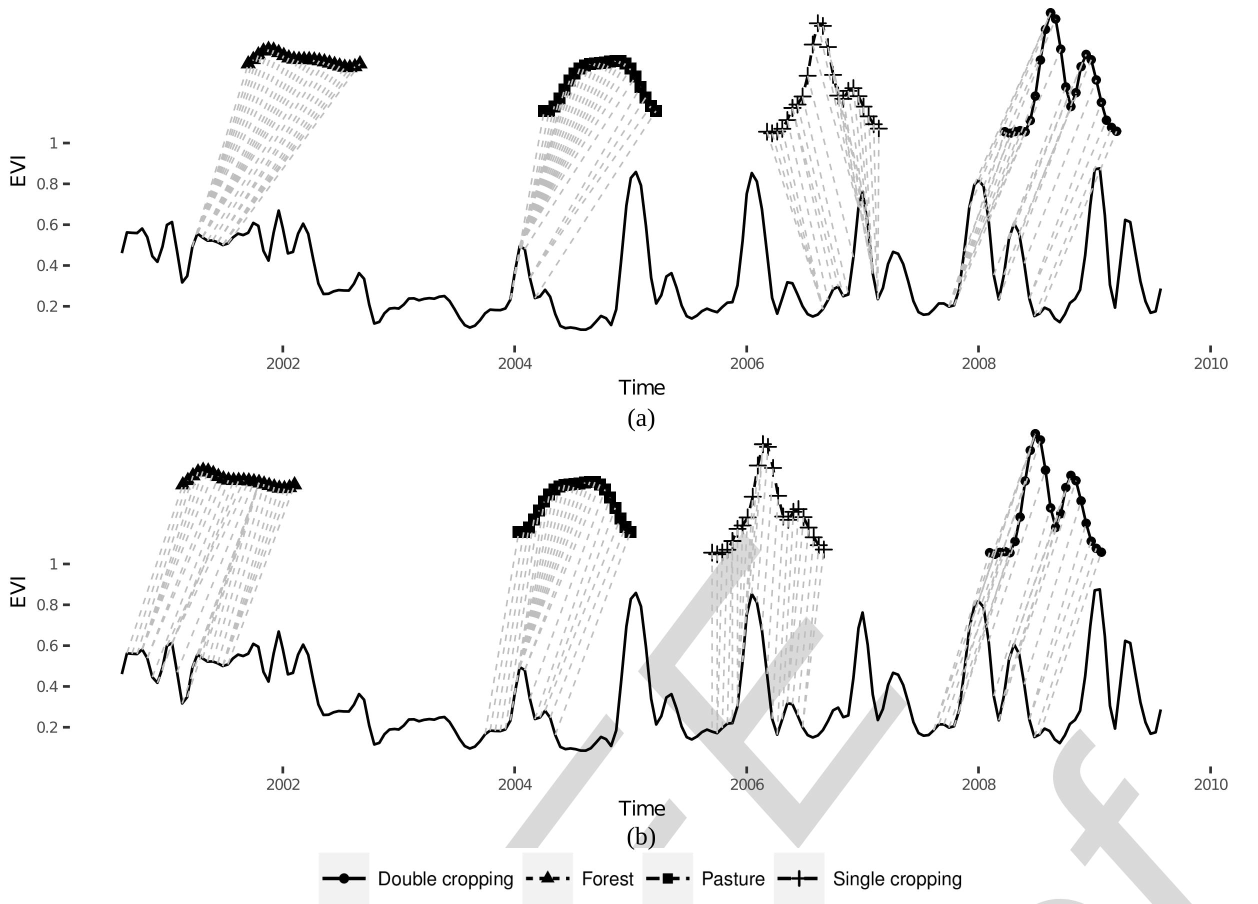

Fig. 7. Best matches of forest, pasture, single cropping, and double cropping to a sample time series using DTW without time restriction in (a), and the time-weighted DTW in (b).

TABLE I
ACCURACY ASSESSMENT FOR EACH CLASS BASED ON 489 REFERENCE SAMPLES CLASSIFIED FROM THE LANDSAT IMAGES

Method	Double cropping		Forest		Pasture		Single cropping	
	User (%)	Producer (%)	User (%)	Producer (%)	User (%)	Producer (%)	User (%)	Producer (%)
DTW without time restrictions	74.65	46.09	88.51	72.64	79.53	80.47	50.00	77.78
DTW with maximum delay of 100 days	88.89	90.43	93.00	87.74	88.20	84.02	72.82	75.76
Linear TWDTW	96.70	76.52	96.81	85.85	83.54	78.11	60.27	88.89
Logistic TWDTW for $\alpha = 0.1$ and $\beta = 100$ days	92.04	90.43	94.00	88.68	88.41	85.80	75.00	84.85

a class called cropland. Other MODIS classes are less than 0.008% of the pixels in this area, and thus they were not considered in this paper.

The accuracy assessment comparing logistic TWDTW results and MODIS land cover is shown in Table IV. The TWDTW algorithm had a global accuracy of 91.21%, better than the global accuracy of MODIS (79.36%). TWDTW had higher user's and producer's accuracies than the MODIS classification for all classes. Although, MODIS had high user accuracy for forest (87.2%) and cropland (89.33%), its *producer's* accuracy for these classes was low (77.37% and 75.28%, respectively).

We compared our forest area with estimations by the Amazon Monitoring Program PRODES [35]. To be able to compare results with the pristine forest area that comes from PRODES, we need to split our "forest" class into "pristine forest" and "secondary vegetation." This requires a land-cover transition rule. Areas matching a forest pattern were classified as forest only if they had also been classified as forest in previous years. Otherwise, we classified them as secondary vegetation. For the first year of the time series, the areas matching a forest pattern are classified as forest. There is no secondary vegetation in the first year of our classification. Using this rule, we got a class of "pristine forest" that is comparable to the PRODES dataset.

Since it is difficult to distinguish secondary vegetation from primary forest using visual interpretation of Landsat images, we joined these two classes to forest in the accuracy assessment. The total forest (pristine forest) and the secondary vegetation areas are presented in Fig. 8. The forest area estimated using the logistic TWDTW is in line with the area estimated by PRODES [35]. Most of the deforestation occurred before 2005, which was followed by an increase of the secondary vegetation area in 2007.

TABLE II
CONFUSION MATRICES BASED ON 489 REFERENCE SAMPLES CLASSIFIED FROM THE LANDSAT IMAGES

	Reference			
Predicted	Double cropping	Forest	Pasture	Single cropping
DTW without time restrictions				
Double cropping	53	2	4	12
Forest	0	77	7	3
Pasture	5	25	136	5
Single cropping	57	1	19	77
Unclassified	0	1	3	2
DTW with maximum delay of 100 days				
Double cropping	104	1	1	11
Forest	0	93	7	0
Pasture	2	11	142	6
Single cropping	9	1	18	75
Unclassified	0	0	1	7
Linear TWDTW				
Double cropping	88	0	0	3
Forest	0	91	3	0
Pasture	3	15	132	8
Single cropping	24	0	34	88
Unclassified	0	0	0	0
Logistic TWDTW for $\alpha = 0.1$ and $\beta = 100$ days				
Double cropping	104	0	0	9
Forest	0	94	6	0
Pasture	1	12	145	6
Single cropping	10	0	18	84
Unclassified	0	0	0	0

TABLE III
EQUIVALENT CLASSES FOR COMPARISON BETWEEN THE TWDTW CLASSIFICATION AND MODIS LAND-COVER COLLECTION 5, PLANT FUNCTIONAL TYPE (PFT)

Aggregated	MODIS PFT	TWDTW
Forest	Evergreen Needleleaf trees, Evergreen Broadleaf trees, and Deciduous Broadleaf trees	Forest, and secondary vegetation
Pastureland	Shrub and grass	Pasture
Cropland	Cereal crops, and broad-leaf crops	Single cropping and double cropping

TABLE IV
ASSESSMENT OF MODIS COLLECTION 5 PLANT FUNCTIONAL TYPE (PFT) AND LOGISTIC TWDTW BASED ON 489 REFERENCE SAMPLES CLASSIFIED FROM THE LANDSAT IMAGES

	User (%)		Producer (%)	
Class	MODIS	TWDTW	MODIS	TWDTW
Forest	87.23	94.00	77.36	88.68
Pastureland	67.71	88.41	85.53	85.80
Cropland	89.33	92.00	75.28	96.73

The classes forest, pastureland, and cropland were aggregated according to Table III.

We also compared our estimated cropland area with the yearly Municipal Agricultural Production Survey (PAM) from 2001 to 2013 done by the Brazilian Census Bureau (IBGE) [38]. The PAM survey provides the information on planted area, harvested area, amount produced, average yield, and production value of permanent and temporary crops by municipality. Since PAM is a sampling survey and not a comprehensive census, some municipalities, especially those in the Brazilian Amazon, can have significant inter-annual variations.

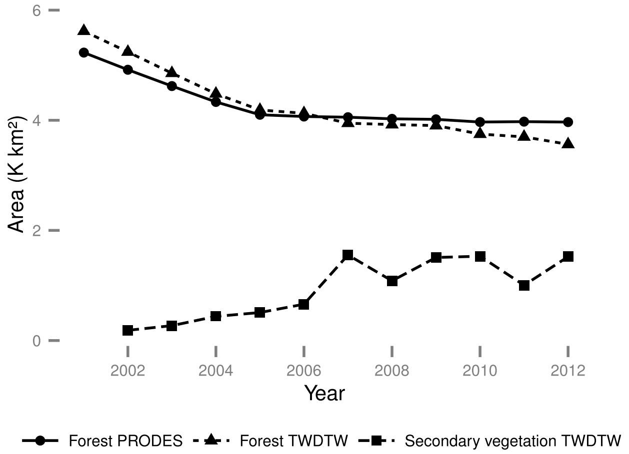

Fig. 8. Forest area estimated by the Amazon Monitoring Program PRODES [35] and using the logistic TWDTW-based classification for Porto dos Gaúchos.

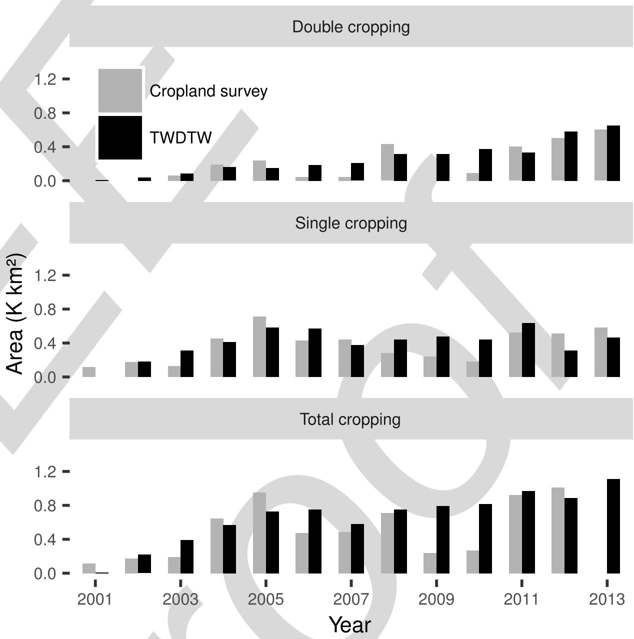

Fig. 9. Total area of double cropping and single cropping in Porto dos Gaúchos estimated by TWDTW and the Brazilian national cropland survey [38].

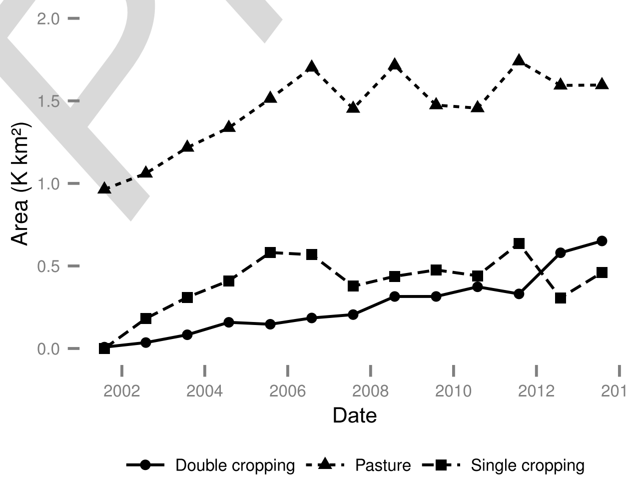

Fig. 10. Total area of pasture, single cropping, and double cropping from 2001 to 2013 estimated using logistic TWDTW for Porto dos Gaúchos.

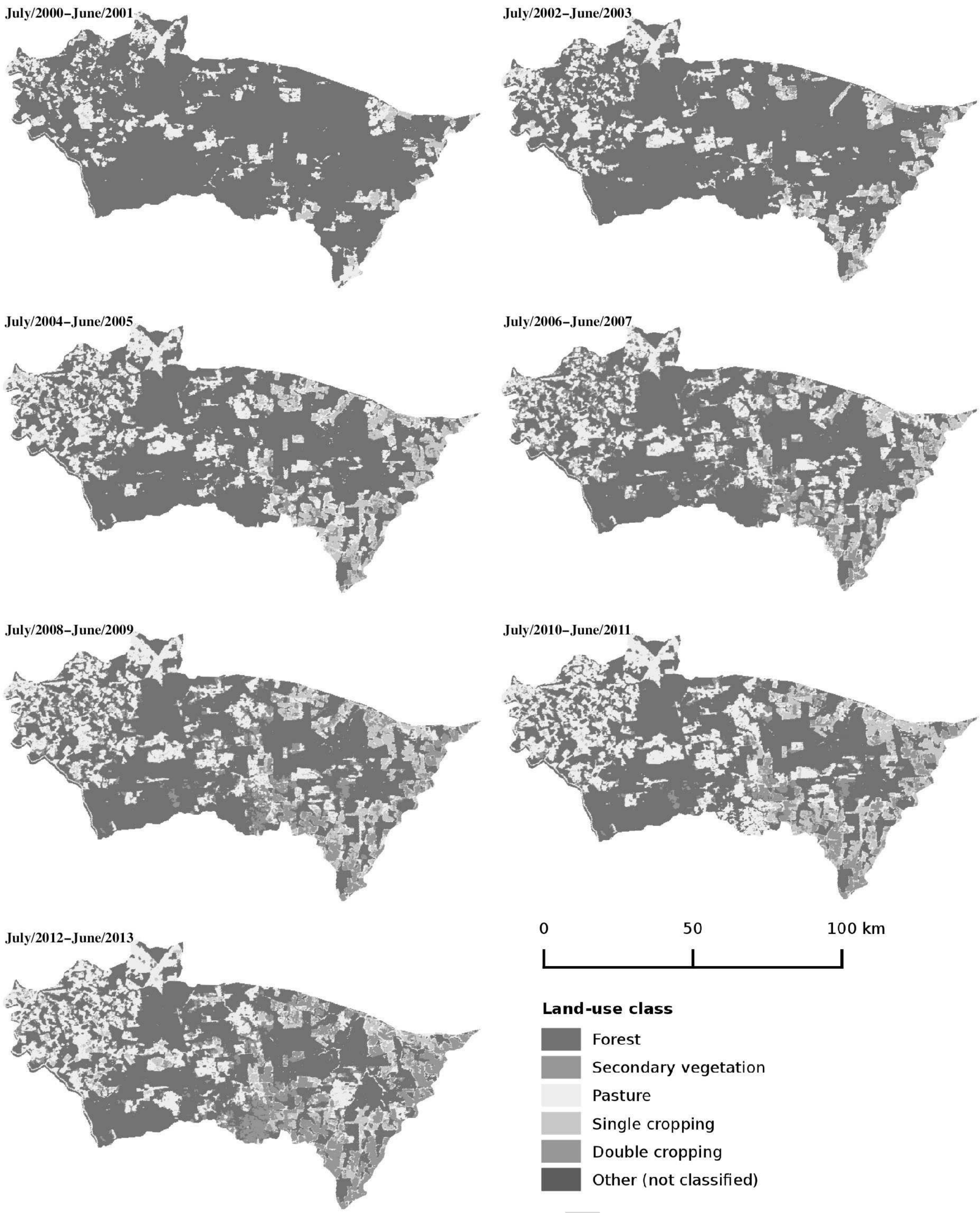

Fig. 11. Land-use/cover maps produced by using the logistic TWDTW classification. Each map shows the classification for an agricultural year (from July to June) in Porto dos Gaúchos.

We use the PAM because it is the only survey that is available yearly for the period 2000 to 2013. Fig. 9 shows the area of single cropping and double cropping estimated by using the logistic TWDTW algorithm and the Brazilian national cropland survey [38] for Porto dos Gaúchos. There is a general agreement between our results and the crop surveys, except in the years 2009 and 2010.

The total agricultural areas (pasture, single cropping, and double cropping) are shown in Fig. 10. In the time series, the pasture and single cropping areas were increasing until 2006, while the double cropping area has a growing trend during the whole period. In the last 2 years of the time series, the double cropping exceeded the single cropping area.

Fig. 11 shows the spatial distribution of land use and land cover in Porto dos Gaúchos for each second agricultural year from 2001 to 2013. In the last decade, a cropland intensification has happened in the Eastern part of Porto dos Gaúchos while pasture expansion has taken place in the Western part.

V. Discussion

Our results show that it pays to have a flexible approach to temporal restrictions when using DTW for land-cover and land-use classification. The original DTW method disregards the temporal range when finding the best alignment between two time series. This precludes an accurate land-use and land-cover classification. The time constraints included in the TWDTW similarity measure should be flexible to handle with the small phase changes related to natural phenological variability.

The maximum time delay, proposed by [13], is flexible for small time warps. However, it forces the dynamic algorithm, (5), to map the warping path inside of a limiting time window that can preclude the classification of some areas (cf. unclassified samples in Table II).

A large cost for small time warps, as the linear TWDTW method does, harms the classification and reduces its sensitivity. The linear TWDTW had low *producer's accuracy*, respectively, 78.11%, 76.52%, when classifying pasture and double cropping (cf. Table I).

The DTW without time restriction had the worst results. More than half of the areas of double cropping were classified as single cropping. These errors come from the over warping of single cropping to fit the first growing season of the double cropping occurrences, cf. Fig. 7(a).

The logistic TWDTW had better results for these land-use classes, because of its low penalty for small time warps and its significant costs for large time warps. Its better accuracy derives from its flexibility to find the best match between a pattern and an interval within a long-term time series.

When comparing our cropland estimated area with data from the yearly Municipal Agricultural survey [38], our results generally match, except for 2009 and 2010 (Fig. 9). In the PAM, the large variations between 2008 and 2009 and between 2010 and 2011 are difficult to explain. Since this is a region of large-scale crop production, one would not expect such a large variation. This fact indicates that remote sensing time-series analysis can complement and add value to cropland surveys such as PAM.

The forest area estimated using the logistic TWDTW was similar to the forest area from the INPE's Amazon Monitoring system (PRODES) (Fig. 8). However, our algorithm had higher estimates for the forest area until 2006 and lower estimates for subsequent years. The higher forest area estimated by the logistic TWDTW compared to PRODES in the first years of the time series is likely related to their different scale of analysis. While we used MODIS images with 250-m spatial resolution the PRODES project uses 30-m Landsat images. Therefore, PRODES is capable of detecting deforestation in small areas that may not be detected at the MODIS resolution.

In the second part of the graphic in Fig. 8, the lower forest area estimated by our method was caused by the transition rule used in our algorithm to separate the secondary vegetation from

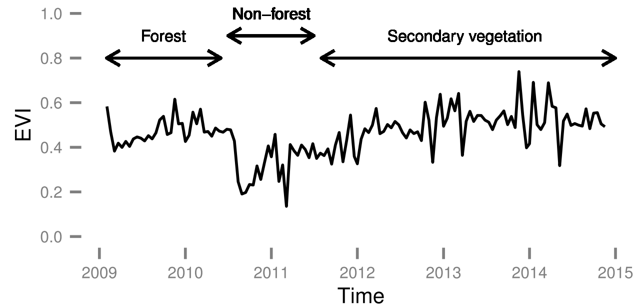

Fig. 12. Example of a classification using the transition rules. This is a sample time series inside of a burned area. This area was degraded in 2011 according to the Detection of Forest Degradation Program (DEGRAD) [43].

the forest. Applying this rule, an area that changes from forest to any other land class cannot become forest again. For example, after a degradation event (e.g., by fire), the area is classified as secondary vegetation in our algorithm, cf. Fig. 12. Therefore, our estimation reduces from the forest area both deforested and degraded areas, whereas PRODES reduces from the forest area only the deforestation by clear-cutting, i.e., it reduces the forest area only when most or all the trees are uniformly removed.

One current challenge for large-scale application of TWDTW algorithm is its computational time. The implementation of the TWDTW algorithm was developed in R [44], [45] using the package dtw [46]. Our case study in Porto dos Gaúchos has 130 500 time series, each with 300 points. The computation time was around 50 min for all DTW variations on a server using 40 cores with 2.6-GHz clock and 256-GB memory. We expect that recent developments on specialized software such as array databases [47], coupled with hardware advances, and better indexing strategies will improve performance considerably.

VI. Conclusion

This paper presents a version of the DTW algorithm suitable for land-use and land-cover classification of remote sensing time series. Refinements to standard DTW include a temporal restriction that allows for phase-shifts due to seasonal changes of natural and cultivated vegetation types. In a tropical forest area, the method has a high accuracy for mapping classes of single cropping, double cropping, forest, and pasture.

Accuracy assessments show the method compares favorably to other DTW variations for land classification. The logistic TWDTW had better results than the other tested alternatives with a global accuracy of 87.32%. Our classification using the logistic TWDTW has higher accuracy and spatial resolution than the MODIS land-cover product. Forest and cropland areas are in line with the Amazon Monitoring Program PRODES and with the Brazilian national cropland surveys, respectively. These results highlight the potential of the TWDTW to improve land-use and land-cover products and contribute to agricultural statistics.

We expect that the TWDTW algorithm will be successful for large-scale land-cover classification of remote sensing time series, if some conditions are met. If the spatial and temporal resolutions of the data are adequate to capture the properties of the landscape, and the samples express the temporal variations of the land-cover types, TWDTW has many advantages. Its flexibility for warping a temporal signature is useful to account for natural and cultivated vegetation types even with inter-annual climatic and seasonal variability.

The proposed method is pixel-based. We envisage future versions that include local neighborhoods to reduce border effects and improve classification homogeneity. Given that the DTW algorithm produces a distance measure between each interval of a long-term time series and all the temporal patterns, these measures could be used as a prior probability estimation for a Bayesian postclassification produce that borrows information from the neighbors.

Postprocessing rules can improve TDWTW results. In this paper, we show how to use rules to distinguish pristine forest from forest regrowth. Using appropriate rules, it is also possible to apply the method for forest degradation, real-time change detection, and crop-condition assessments.

The results in this paper have been obtained using only the EVI time-series signal. We expect further improvements using multiband time series, including the original spectral bands and transformed ones such as NDVI, EVI, and spectral unmixed endmembers.

The TWDTW algorithm is suitable for applications of remote sensing time series where the temporal variation is more important than the spatial variation for classifying remote sensing datasets. These cases include areas of large farms, such as those found in Brazil. For urban areas with less seasonal change or areas with small farms, it is likely that time warping methods need to be combined with object-based image analysis for accurate classification of the landscape.

REFERENCES

[1] S. Fritz *et al.*, "The need for improved maps of global cropland," *Eos Trans. Amer. Geophys. Union*, vol. 94, no. 3, pp. 31–32, 2013.

[2] G. J. Roerink, M. Menenti, and W. Verhoef, "Reconstructing cloudfree NDVI composites using Fourier analysis of time series," *Int. J. Remote Sens.*, vol. 21, no. 9, pp. 1911–1917, 2000.

[3] R. S. Lunetta, J. F. Knight, J. Ediriwickrema, J. G. Lyon, and L. D. Worthy, "Land-cover change detection using multi-temporal MODIS NDVI data," *Remote Sens. Environ.*, vol. 105, no. 2, pp. 142–154, 2006.

[4] J. Verbesselt, R. Hyndman, G. Newnham, and D. Culvenor, "Detecting trend and seasonal changes in satellite image time series," *Remote Sens. Environ.*, vol. 114, no. 1, pp. 106–115, 2010.

[5] J. Verbesselt, A. Zeileis, and M. Herold, "Near real-time disturbance detection using satellite image time series," *Remote Sens. Environ.*, vol. 123, pp. 98–108, 2012.

[6] P. Jönsson and L. Eklundh, "Seasonality extraction by function fitting to time-series of satellite sensor data," *IEEE Trans. Geosci. Remote Sens.*, vol. 40, no. 8, pp. 1824–1832, Aug. 2002.

[7] P. Griffiths, S. van der Linden, T. Kuemmerle, and P. Hostert, "A pixel-based Landsat compositing algorithm for large area land cover mapping," *IEEE J. Sel. Topics Appl. Earth Observ. Remote Sens.*, vol. 6, no. 5, pp. 2088–2101, Oct. 2013.

[8] R. E. Kennedy, Z. Yang, and W. B. Cohen, "Detecting trends in forest disturbance and recovery using yearly Landsat time series: 1. LandTrendr—Temporal segmentation algorithms," *Remote Sens. Environ.*, vol. 114, no. 12, pp. 2897–2910, 2010.

[9] Z. Zhu, C. E. Woodcock, and P. Olofsson, "Continuous monitoring of forest disturbance using all available Landsat imagery," *Remote Sens. Environ.*, vol. 122, no. 0, pp. 75–91, 2012, Landsat Legacy Special Issue.

[10] B. DeVries, J. Verbesselt, L. Kooistra, and M. Herold, "Robust monitoring of small-scale forest disturbances in a tropical montane forest using Landsat time series," *Remote Sens. Environ.*, vol. 161, pp. 107–121, 2015.

[11] X. Xiao *et al.*, "Mapping paddy rice agriculture in southern china using multi-temporal MODIS images," *Remote Sens. Environ.*, vol. 95, no. 4, pp. 480–492, 2005.

[12] B. D. Wardlow, S. L. Egbert, and J. H. Kastens, "Analysis of time-series MODIS 250 m vegetation index data for crop classification in the U.S. Central Great Plains," *Remote Sens. Environ.*, vol. 108, no. 3, pp. 290–310, 2007.

[13] F. Petitjean, J. Inglada, and P. Gancarski, "Satellite image time series analysis under time warping," *IEEE Trans. Geosci. Remote Sens.*, vol. 50, no. 8, pp. 3081–3095, Aug. 2012.

[14] G. le Maire, S. Dupuy, Y. Nouvellon, R. A. Loos, and R. Hakamada, "Mapping short-rotation plantations at regional scale using MODIS time series: Case of eucalypt plantations in Brazil," *Remote Sens. Environ.*, vol. 152, no. 0, pp. 136–149, 2014.

[15] G. L. Galford, J. F. Mustard, J. Melillo, A. Gendrin, C. C. Cerri, and C. E. Cerri, "Wavelet analysis of MODIS time series to detect expansion and intensification of row-crop agriculture in Brazil," *Remote Sens. Environ.*, vol. 112, no. 2, pp. 576–587, 2008.

[16] T. Sakamoto, P. C. Van Kotera, K. D. Nguyen, and M. Yokozawa, "Analysis of rapid expansion of inland aquaculture and triple rice-cropping areas in a coastal area of the Vietnamese Mekong Delta using MODIS time-series imagery," *Landscape Urban Plann.*, vol. 92, no. 1, pp. 34–46, 2009.

[17] D. J. Berndt and J. Clifford, "Using dynamic time warping to find patterns in time series," in *Proc. KDD Workshop*, 1994, pp. 359–370.

[18] P. Esling and C. Agon, "Time-series data mining," *ACM Comput. Surv.*, vol. 45, no. 1, pp. 12:1–12:34, Dec. 2012.

[19] T. Rakthanmanon *et al.*, "Searching and mining trillions of time series subsequences under dynamic time warping," in *Proc. 18th ACM SIGKDD Int. Conf. Knowl. Discov. Data Min.*, 2012, pp. 262–270.

[20] V. Velichko and N. Zagoruyko, "Automatic recognition of 200 words," *Int. J. Man-Mach. Stud.*, vol. 2, no. 3, pp. 223–234, 1970.

[21] H. Sakoe and S. Chiba, "A dynamic programming approach to continuous speech recognition," in *Proc. 7th Int. Congr. Acoust. Budapest*, 1971, vol. 3, pp. 65–69.

[22] H. Sakoe and S. Chiba, "Dynamic programming algorithm optimization for spoken word recognition," *IEEE Trans. Acoust. Speech Signal Process.*, vol. 26, no. 1, pp. 43–49, Feb. 1978.

[23] L. Rabiner and B.-H. Juang, *Fundamentals of Speech Recognition*. Englewood Cliffs, NJ, USA: Prentice-Hall, 1993.

[24] E. Keogh and C. A. Ratanamahatana, "Exact indexing of dynamic time warping," *Knowl. Inf. Syst.*, vol. 7, no. 3, pp. 358–386, 2005.

[25] Y.-S. Jeong, M. K. Jeong, and O. A. Omitaomu, "Weighted dynamic time warping for time series classification," *Pattern Recognit.*, vol. 44, no. 9, pp. 2231–2240, 2011.

[26] B. C. Reed, J. F. Brown, D. VanderZee, T. R. Loveland, J. W. Merchant, and D. O. Ohlen, "Measuring phenological variability from satellite imagery," *J. Veg. Sci.*, vol. 5, no. 5, pp. 703–714, 1994.

[27] X. Zhang *et al.*, "Monitoring vegetation phenology using MODIS," *Remote Sens. Environ.*, vol. 84, no. 3, pp. 471–475, 2003.

[28] F. Petitjean and J. Weber, "Efficient satellite image time series analysis under time warping," *IEEE Geosci. Remote Sens. Lett.*, vol. 11, no. 6, pp. 1143–1147, Jun. 2014.

[29] M. Müller, *Information Retrieval for Music and Motion*. New York, NY, USA: Springer, 2007.

[30] A. Huete, H. Liu, K. Batchily, and W. van Leeuwen, "A comparison of vegetation indices over a global set of TM images for EOS-MODIS," *Remote Sens. Environ.*, vol. 59, no. 3, pp. 440–451, 1997.

[31] A. Huete, K. Didan, T. Miura, E. Rodriguez, X. Gao, and L. Ferreira, "Overview of the radiometric and biophysical performance of the MODIS vegetation indices," *Remote Sens. Environ.*, vol. 83, nos. 1–2, pp. 195–213, 2002.

[32] R. M. de Freitas *et al.*, "Virtual laboratory of remote sensing time series: Visualization of MODIS EVI2 data set over South America," *J. Comput. Interdiscip. Sci.*, vol. 2, no. 1, pp. 57–68, 2011.

[33] S. Mallat, *A Wavelet Tour of Signal Processing*, 2nd ed. San Diego, CA, USA: Academic, 1998.

[34] T. Sakamoto, M. Yokozawa, H. Toritani, M. Shibayama, N. Ishitsuka, and H. Ohno, "A crop phenology detection method using time-series MODIS data," *Remote Sens. Environ.*, vol. 96, nos. 3–4, pp. 366–374, 2005.

[35] INPE (National Institute for Space Research, Brazil). (2014). *Amazon Deforestation Monitoring Project—PRODES* [Online]. Available: www.obt.inpe.br/prodes

[36] A. P. D. Aguiar, G. Câmara, and M. I. S. Escada, "Spatial statistical analysis of land-use determinants in the Brazilian Amazonia: Exploring intra-regional heterogeneity," *Ecol. Model.*, vol. 209, nos. 2–4, pp. 169–188, 2007.

[37] INPE (National Institute for Space Research, Brazil). (2008). *Amazon Land Use Database—TerraClass* [Online]. Available: www.inpe.br/cra/projetos_pesquisas/terraclass2008/
[38] IBGE (Brazilian Institute of Geography, and Statistics). (2014). *Municipal Agricultural Production—PAM* [Online]. Available: www.sidra.ibge.gov.br/bda/
[39] D. Arvor and M. Jonathan, M. S. o. P. Meirelles, V. Dubreuil, and L. Durieux, "Classification of MODIS EVI time series for crop mapping in the state of Mato Grosso, Brazil," *Int. J. Remote Sens.*, vol. 32, no. 22, pp. 7847–7871, 2011.
[40] R. G. Aguiar, C. V. Randow, N. P. Filho, A. O. Manzi, L. J. G. Aguiar, and F. L. Cardoso, "Fluxos de massa e energia em uma floresta tropical no sudoeste da amazônia," *Braz. J. Meteorol.*, vol. 21, no. 3b, pp. 248–257, 2006.
[41] Google. (2014). *Google Earth Engine* [Online]. Available: https://earthengine.google.org/
[42] M. A. Friedl *et al.*, "Modis collection 5 global land cover: Algorithm refinements and characterization of new datasets," *Remote Sens. Environ.*, vol. 114, no. 1, pp. 168–182, 2010.
[43] INPE (National Institute for Space Research, Brazil). (2014). *Detection of Forest Degradation (DEGRAD)* [Online]. Available: www.obt.inpe.br/degrad/
[44] R. Ihaka and R. Gentleman, "R: A language for data analysis and graphics," *J. Comput. Graph. Statist.*, vol. 5, no. 3, pp. 299–314, 1996.
[45] R Core Team, *R: A Language and Environment for Statistical Computing*, Version 3.2.3, R Foundation for Statistical Computing, Vienna, Austria, 2015 [Online]. Available: https://www.R-project.org/
[46] T. Giorgino, "Computing and visualizing dynamic time warping alignments in R: The DTW package," *J. Statist. Softw.*, vol. 31, no. 7, pp. 1–24, 2009.
[47] M. Stonebraker, P. Brown, D. Zhang, and J. Becla, "SciDB: A database management system for applications with complex analytics," *Comput. Sci. Eng.*, vol. 15, no. 3, pp. 54–62, 2013.

Victor Maus (S'15–M'16) was born in Formigueiro, Brazil. He received the B.Sc. degree in environmental engineering from the Franciscan University Center, Brazil, in 2009, and the M.Sc. degree in computational modeling from the Federal University of Juiz de Fora, Brazil, in 2011.

Currently, he is a Ph.D. candidate in earth system science at Brazil's National Institute for Space Research (INPE), São José dos Campos, Brazil, and works as an assistant researcher at the Institute for Geoinformatics (IFGI), University of Münster, Germany. His research interests include scientific computing, numerical analysis, environmental applications, and land use changes.

Gilberto Câmara received the Ph.D. degree in computer science from Brazil's National Institute for Space Research (INPE), São José dos Campos, Brazil, in 1995.

He has been a Researcher and a Professor of Geoinformatics, Spatial Databases, and Land Use Change with INPE, where he was the General Director (2006–2012).

Dr. G. Câmara was a Brazil Chair at the Institute for Geoinformatics, University of Münster, Münster, Germany, from 2013 to 2015. He advised 50 graduate students and authored 150 papers that have been cited more than 7500 times. He was a recipient of the Dr. Honoris Causa from the University of Muenster, and the William T. Pecora Award from NASA and USGS for "leadership to the broad and open access to remote sensing data."

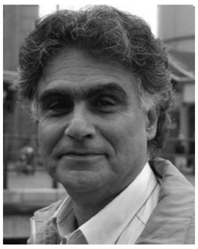

Ricardo Cartaxo received the B.Sc. degree in electronic engineering from the Technological Institute of Aeronautics (ITA), Brazil, in 1975.

He is a Senior Engineer with the Earth Observation Directorate at Brazil's National Institute for Space Research (INPE), São José dos Campos, Brazil, and Chief Architect of INPE's Geospatial Technologies. He has 30 years of experience in remote sensing image processing and geospatial software development.

Alber Sanchez received the B.Sc. degree in cadastre and geodesy and the M.Sc. degree in information and communication sciences from the District University of Bogotá, Bogotá, Colombia, in 2001 and 2007, respectively, and the M.Sc. degree in geoInformatics from the University of Münster, Münster, Germany, in 2013. Currently, he is pursuing the Ph.D. degree in earth system science at the Institute for Space Research (INPE), São José dos Campos, Brazil.

His research interests include the use of distributed array databases for processing large amounts of Earth observation data.

Fernando M. Ramos received the Ph.D. degree in fluid mechanics from National Higher School of Aeronautics and Space (ENSAE), France, in 1992.

He is a Senior Researcher with the Computing and Applied Mathematics Laboratory at Brazil 's National Institute for Space Research (INPE), São José dos Campos, Brazil. His research interests include scientific computing, time-series analysis, inverse problems, complex systems modeling and simulation, in applications that range from Meteorology to Remote Sensing and Geophysics. During the past decade, he has been the principal investigator at INPE of several national and international research projects and represented Brazil, as seconded expert, at the Group on Earth Observations (GEO), Geneva.

Gilberto R. de Queiroz was born in Belo Horizonte, Brazil, on December 30, 1976. He received the M.Sc. and Ph.D. degrees in applied computing from the Institute for Space Research (INPE), São José dos Campos, Brazil, in 2003 and 2012, respectively.

Since 2005, he has been a System Engineer and Professor of Spatial Databases with INPE, focused on the development of geo-technology.